One-dimensional electron localization in semiconductors coupled to electromagnetic cavities

Dmitry Svintsov,* Georgy Alymov, and Zhanna Devizorova
Moscow Institute of Physics and Technology, Dolgoprudny 141700, Russia

Luis Martin-Moreno†
Instituto de Nanociencia y Materiales de Aragon (INMA), CSIC-Universidad de Zaragoza, Zaragoza 50009, Spain and Departamento de Fisica de la Materia Condensada, Universidad de Zaragoza, Zaragoza 50009, Spain

(Received 2 December 2022; revised 28 December 2023; accepted 5 January 2024; published 24 January 2024)

The electrical conductivity of one-dimensional (1D) disordered solids exhibits exponential decay with respect to their length, a well-known manifestation of the localization phenomenon. In this study, we investigate alterations in the conductivity resulting from the insertion of 1D semiconductors into single-mode electromagnetic cavities, focusing specifically on the regime of nondegenerate doping. Our approach employs the Green's function technique adapted for the nonperturbative consideration of cavity-excited states. This encompasses coherent electron-cavity effects, such as electron motion within the zero-point fluctuating field, as well as incoherent photon emission processes during tunneling. The energy spectrum of electron transmission across the cavity develops Fano-type resonances linked to virtual photon emission, passage along a resonant level, and photon reabsorption. The quality factor of the Fano resonance depends on whether the intermediate state is coupled to the leads, reaching its maximum when this state is deeply localized within the disorder potential. Coupling to the cavity also raises the energies of shallow bound states, bringing them close to the conduction band bottom. This effect results in an enhancement of the conductance at low temperatures.

DOI: 10.1103/PhysRevB.109.045432

I. INTRODUCTION

The exploration of manifestations stemming from the nonempty electromagnetic vacuum in measurable real-life phenomena has been a focal point of research since the inception of quantum field theory [1–3]. Historically, most observed manifestations, such as the electron's anomalous magnetic moment and the Lamb shift, have been confined to the realm of atomic physics. Recent advances in the fabrication of high-quality electromagnetic cavities [4], coupled with the discovery of ultra-confined electromagnetic waves [5,6], have given rise to the intriguing concept of manipulating the macroscopic properties of matter through zero-point oscillations [7–13]. Remarkable experimental examples include the manipulating of superconducting critical temperatures with cavities [14] and the modification of chemical reaction rates [15]. Nonetheless, changing the conductivity of solids, the property of primary interest in electronics, has been traditionally deemed implausible even under resonant coupling [16]. Indeed, the momentum an electron acquires in a zero-point vacuum field is much less than thermal or Fermi momentum at achievable temperatures and carrier densities.

Recent experiments have challenged this perspective. Ref. [17] demonstrated cavity-enhanced conductivity in a disordered organic semiconductor adjacent to a photonic crystal. Reference [18] showcased the impact of microwave cavities on the magnetoresistance of quantum wells. Subsequent investigations of analogous systems revealed a finite dissipative conductivity on the fractional quantum Hall plateaus [19]. Reference [20] uncovered the existence of strong photocurrent in the level anticrossing gap induced by an optical cavity. The intricacy of these experiments lies in comparing sample properties with and without a cavity, a task complicated by non-equivalent disorder, intrinsic fields, and geometric variations. It is thus intriguing to theoretically elucidate the conditions under which the conductivity of solids may vary due to electromagnetic cavities. Once these conditions are identified, the incorporation of cavities could emerge as a novel turning knob for manipulating electrical properties, complementing traditional approaches such as doping and field effects.

In this study, we demonstrate that a particularly suitable playground for pronounced manifestations of zero-point electromagnetic oscillations, even under weak coupling, is found in one-dimensional (1D) disordered conductors operating within the localized regime [21,22].

Previous works primarily focused on transport in cavity-coupled ordered systems [23–28], or cavity modifications of individual scattering events [29,30]. In 1D systems electrically decoupled from the leads, the impact of the cavity field on the localization length was observed to be oscillatory under strong coupling conditions [31]. Recently, Refs. [32,33] presented studies on conductance and the quantum Hall effect in cavity-coupled disordered 1D and 2D systems in the case of degenerate doping. They argued for the emergence

*svintcov.da@mipt.ru
†lmm@unizar.es

 ©2024 American Physical Society

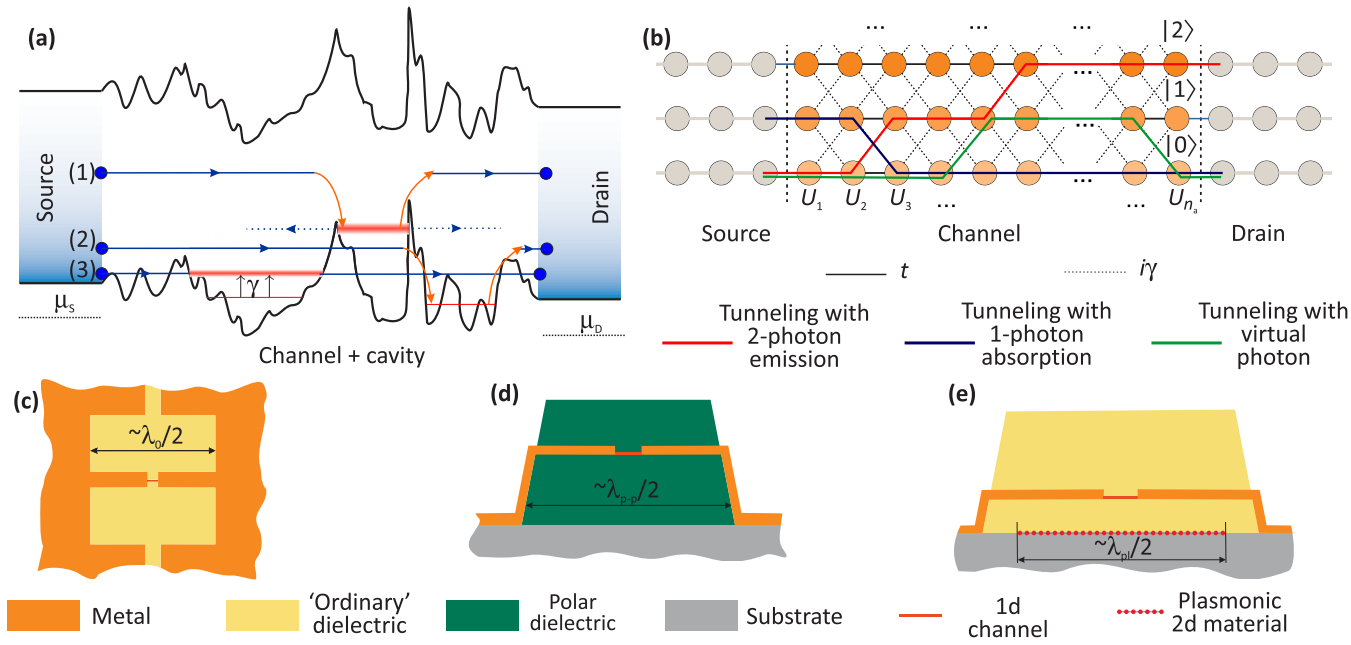

FIG. 1. One-dimensional disordered semiconductor in a cavity. (a) Mechanisms of conduction modifications via electromagnetic cavity fluctuations (1) An electron can emit a virtual photon, travel along an electronic quasibound resonant level, and reabsorb the photon. The quasi-bound level is susceptible to decay into source and drain, resulting in electroluminescence (2) Similar to (1), but an electron is genuinely bound in the disorder potential, precluding luminescence (3) The coupling of the conductor to a cavity with strength γ induces the expulsion of the shallow bound states from the disorder potential. Consequently, new resonances may appear in the transmittance (b) Extended states' space for a tight-binding chain strongly coupled to a cavity mode. Each atomic site with potential U_i is now characterized by a number of cavity photons $|N\rangle$, as do the states in the leads. Different-colored paths represent various possibilities of source-drain tunneling. Green: elastic tunneling perturbed by emission/absorption of virtual photons, blue: tunneling with single photon absorption, red: tunneling with two-photon emission. (c)–(e) Examples of electromagnetic cavities where the effects under study can take place (c) microwave slot resonator of size order of free-space wavelength λ_0 (d) cavity based on a polar dielectric with size order of phonon-polariton wavelength λ_{p-p} (e) 2D plasmonic cavity based on a 2D material supporting confined 2D plasmons with wavelength λ_p.

of cavity-induced long-range electron hopping. The complexity of this regime stems from the Pauli blocking of electronic states following the emission of cavity photons. These effects can be accurately addressed only through Keldysh Green's function technique. This has been applied to related systems, such as molecular transistors strongly coupled to phononic vibrations [34,35]. Unfortunately, extending this technique to ultrastrong coupling proves challenging due to the complex nature of diagrammatic expressions for electron-photon self-energies.

In this work, we focus on the conductivity of *non-degenerate* disordered 1D semiconductors coupled to single-mode cavities. The low fermionic occupation numbers $n_F \ll 1$ allow us to disregard Pauli blocking effects, enabling a numerical and nonperturbative treatment of electron-cavity couplings. The absence of Pauli blocking uncovers strong coupling effects, primarily — but not exclusively —involving the emission of virtual photons during transport. From an experimental viewpoint, the nondegenerate regime is realized in intrinsic and moderately doped semiconductors, always achievable through gating.

We find that coupling a one-dimensional semiconductor to a cavity results in resonances in the electron transmission $\mathcal{T}(E)$ at energies corresponding to the multi-photon replicas of quasibound states, $E = E_i + N\hbar\omega$ [process No. (1) in Fig. 1(a)]. The replica resonances in transmission have a Fano-type structure. The probabilities of photon-assisted tunneling have resonances at the same replica energies, albeit having a standard Lorentzian shape. At large photon energies $\hbar\omega \gg kT$, the emergence of such resonances does not lead to any modifications of 1D conductivity. The reason is that such resonances appear at the high energy tail of electron Boltzmann distribution. The situation changes at lower cavity photon energies $\hbar\omega \lesssim kT$ or at relatively large disorder amplitudes $\delta U \gtrsim \hbar\omega$. In such a case, replica resonances may appear near the nominal conduction band edge E_C and significantly contribute to the enhanced conduction. The mechanism of conductivity in this regime represents electron hopping to the true bound state in the disorder potential with virtual photon emission, passage along this state, and subsequent photon absorption [process No. (2) in Fig. 1(a)]. Finally, we find that coupling of disordered 1d wires to cavities can result in the rise of the bound states from the disordered tail to the band, then becoming accessible from the leads [process No. (3) in Fig. 1(a)]. At a coupling strength corresponding to the level unbinding, the thermally-averaged transmittance acquires a resonance.

Our study is based on a modified Landauer-Buttiker formalism in the tight-binding approximation. The non-trivial modification involves the inclusion of cavity degrees of freedom populated according to the thermal Gibbs distribution. The developed method enables the evaluation of both direct

tunnelings modified by the zero-point oscillations of the cavity field and the tunneling aided by the absorption/emission of real photons. Some examples of the relevant processes are shown in Fig. 1(b). Section II will describe the developed theoretical method, while Sec. III will discuss the results on the conductance of disordered 1D chains coupled to the cavities. Section IV explores possible experimental setups where the cavity modifications of conductance can be observed.

II. MODEL: LANDAUER-BUTTIKER APPROACH FOR A TIGHT-BINDING CHAIN IN A CAVITY

A. Hamiltonian of the cavity-coupled chain

The model system under investigation is a 1D atomic chain comprising $n_{\rm at}$ sites. The chain with its contacts is embedded in the electromagnetic cavity with characteristic size $L_{\rm cav}$ of the order of electromagnetic wave length and much exceeding the conductor length. Examples of such cavities are shown in Figs. 1(c)–1(e). These can be metallic slot-type resonators with characteristic size order of free-space photon wavelength [Fig. 1(c)], such cavities are favorable at microwave frequencies [18]. Another example [Fig. 1(d)] is represented by cavities supporting photon-polariton resonances in polar dielectrics such as hexagonal boron nitride [36], such cavities are best combined with 1D systems based on layered semiconductors. The third possible example is represented by 2D plasmonic cavities [5], where the studied 1d conductor is proximized with a 2D material supporting highly confined 2D plasmons [Fig. 1(d)].

Electron transport in the chain is considered within the tight-binding approach, with a constant nearest-neighbor hopping integral t and random on-site energies U_i (Fig. 1). The amplitudes U_i follow an uncorrelated Gaussian distribution with a variance of δU. The electromagnetic field of the single-mode cavity is treated using Pierles' modification of the hopping integrals [27],

$$t \to t\exp\{\pm ieA_x a/\hbar c\}, \tag{1}$$

where A_x is the vector potential along the chain, and a is the lattice constant. As the typical cavity lengths exceed the length of 1D conductors, the vector-potential can be considered as position-independent. In this limit, the quantization rule for the cavity field can be presented as

$$A_x \to A_{\rm vac}(\hat{b} + \hat{b}^+), \tag{2}$$

where $\hat{b}^+$ and $\hat{b}$ are raising and lowering operators for the field, and

$$A_{\rm vac} = \left(\frac{2\pi\hbar c^2}{\omega V}\right)^{1/2} \tag{3}$$

is the amplitude of zero-point oscillations in the cavity of volume V. The quantization rules (2) and (3) imply a single-mode approximation to the cavity spectrum. The lowest-frequency (fundamental) mode of the cavity typically interacts with 1D conductor most strongly. This is justified by the decrease in zero-point amplitude with frequency [Eq. (3)]. Further on, we see that cavity-induced corrections to the energy levels of a disordered conductor are also increasing with lowering the frequency, even at a constant $A_{\rm vac}$.

The above prerequisites lead us to the following Hamiltonian $\hat{\mathcal{H}}$, comprised of a free-field part $\hat{\mathcal{H}}_{\rm f}$ and an interacting chain part $\hat{\mathcal{H}}_{\rm ch}(\gamma)$:

$$\hat{\mathcal{H}} = \hat{\mathcal{H}}_{\rm f} + \hat{\mathcal{H}}_{\rm ch}(\gamma), \tag{4}$$

$$\hat{\mathcal{H}}_{\rm f} = \hbar\omega\hat{b}^+\hat{b}, \tag{5}$$

$$\hat{\mathcal{H}}_{\rm ch}(\gamma) = \sum_{i=1,\pm}^{n_{\rm at}} U_i\hat{a}_i^+\hat{a}_i + te^{\pm\frac{i\gamma}{l}(\hat{b}+\hat{b}^+)}\hat{a}_{i\pm1}^+\hat{a}_i. \tag{6}$$

In the above expression, $\hat{a}_i$, $\hat{a}_i^+$ are fermionic annihilation and creation operators at site i, $\gamma = eatA_{\rm vac}/\hbar c$ is the hopping amplitude associated with photon emission/absorption.

B. Coupling of the interacting chain to the leads

The model chain is connected to source and drain metallic leads, assumed to be noninteracting, and maintained in thermal equilibrium. The effect of the leads on the conductor under study is typically described by the self-energy operator $\hat{\Sigma} = \hat{\Sigma}_s + \hat{\Sigma}_d$, where $\hat{\Sigma}_s$ and $\hat{\Sigma}_d$ govern the effects of source and drain contacts, respectively [37]. Once the functional form of self-energy is specified, all the necessary information about transport is encoded in the propagators (Green's functions) $\hat{G}(E)$. They are determined from

$$\hat{G}(E) = [E\hat{I} - \hat{\mathcal{H}} - \hat{\Sigma}]^{-1}, \tag{7}$$

where E is the energy and $\hat{I}$ is the identity operator.

From this point, our approach to considering electron-boson interactions deviates from conventional diagrammatic expansions of the electron's Green's function in powers of interaction strength [34,35]. We aim at the nonperturbative account of electron-cavity couplings. Therefore, all Green's functions will be defined in the states' space spanned by electron and cavity degrees of freedom. In other words, we will deal with new quasiparticles, electrons dressed in N cavity photons. The state of such quasiparticles is characterized by a multi-index $|\alpha\rangle = |i, N\rangle$, where i is the position in the chain and N is the number of photons in the cavity mode. The energy argument of Green's function E is the total energy of the dressed electron, which, without interactions, comprises the electronic part ε and the photonic part $N\hbar\omega$.

The extended states' space for the dressed electron can now be represented by a 2D network shown in Fig. 1(b). Each horizontal line corresponds to a constant number of cavity photons. Each vertical line corresponds to an electron at a given atomic site, with different possible numbers of photons in the cavity. Importantly, each Nth horizontal line of this network is coupled to the leads, which implies the possibility of inelastic processes, i.e., retaining the cavity in the excited state after the electron passage. The paths between the source and drain across this network have a transparent physical interpretation. For example, the path starting at $|N\rangle = |0\rangle$ and ending at $|M\rangle$, $M \neq 0$ corresponds to an electron entering the cavity in the photonic ground state and leaving the cavity with M excited photons [red line in Fig. 1(b), tunneling with photon emission].

The computation of the Green's function for the compound quantum system (7) requires determining the Hamiltonian and self-energy matrix elements. They are obtained and evaluated

in two steps: initially concerning cavity states and subsequently focusing on electron states. The elements of $\mathcal{H}$ with respect to cavity states, denoted as $\langle M|\hat{\mathcal{H}}|N\rangle$, are analytically computed using the Baker-Campbell-Hausdorff formula (Appendix A). Within a tight-binding subspace, $\mathcal{H}$ is represented by an ordinary tridiagonal matrix.

Obtaining the self-energy operator $\hat{\Sigma}$ for the interacting chain poses a more intricate challenge. This complexity arises from the fact that an electron departing the channel can do so either by maintaining the cavity in its initial state or by emitting/absorbing N cavity photons [Fig. 1(b)]. The rate at which the electron leaves the cavity should depend solely on the electron's energy $\varepsilon = E - N\hbar\omega$. The state of the cavity should not influence the possibility of electron escape. Clearly, an electron cannot exit the cavity if its energy $E - N\hbar\omega$ lies outside the conduction band in the leads. Let us assume that the noninteracting chain's self-energy is known and denoted as $\hat{\Sigma}_0(E)$. The self-energy for the interacting chain, denoted as $\hat{\Sigma}(E)$, satisfying the above requirements, would have the following matrix element with respect to the cavity states:

$$\langle M|\hat{\Sigma}(E)|N\rangle = \delta_{NM}\hat{\Sigma}_0(E - N\hbar\omega). \tag{8}$$

The physical meaning of Eq. (8) becomes clearer when considering that the imaginary part of the self-energy is proportional to the rate of electron escape from the studied system. Mathematically, this can be expressed as $\mathrm{Im}\,\Sigma_0(\varepsilon) \sim \hbar v(\varepsilon)/a$, where $v(\varepsilon)$ is the electron velocity, and a is the interatomic distance. Equation (8) simply represents the fact that emission of N cavity photons reduces the electron velocity from $v(E)$ to $v(E - N\hbar\omega)$, consequently lowering the rate of electron escape from the chain. If $E - N\hbar\omega < 0$, the velocity becomes imaginary, reflecting the energy constraint on the electroluminescence.

After the self-energy for the dressed electron is related to that of a bare electron with Eq. (8), we are left with the specification of the functional form of $\hat{\Sigma}_0 = \hat{\Sigma}_s + \hat{\Sigma}_d$. The general property of this operator is its action only on the terminal atoms in the chain. In other words, the matrices of $\hat{\Sigma}_s$ and $\hat{\Sigma}_d$ in the tight-binding representation have a single nonzero element each. A formal representation of this fact is

$$\langle i|\hat{\Sigma}_s(E)|j\rangle = \delta_{ij}\delta_{i,1}g_s(E), \tag{9}$$

$$\langle i|\hat{\Sigma}_d(E)|j\rangle = \delta_{ij}\delta_{i,n_{\mathrm{at}}}g_d(E). \tag{10}$$

The particular form of scalar coupling functions $g_{s/d}$ on the density of states in the leads and microscopic details of atomic bonds. We adopt the scalar coupling functions $g_{s/d}$ in the simplest approximation of 1D contact with the same bandwidth as the channel [37],

$$g_s(E) = g_d(E) = \frac{2t^2}{E - 2t + i\sqrt{E(4t - E)}}. \tag{11}$$

C. Generalized Landauer formula for the current in the interacting chain

The current I_0 in a non-interacting one-dimensional system biased by voltage $eV_{sd} = \mu_s - \mu_d$ is given by the Landauer formula [38]:

$$I_0 = \frac{2e}{h}\int_{-\infty}^{+\infty} dE[n_F(E) - n_F(E - eV_{sd})]\mathcal{T}_0(E), \tag{12}$$

where $n_F(E)$ are the fermionic occupation numbers. The energy-dependent transmission probability in the non-interacting chain $\mathcal{T}_0(E)$ can be expressed via [39]

$$\mathcal{T}_0 = \mathrm{Tr}[\hat{\Gamma}_S\hat{G}\hat{\Gamma}_D\hat{G}^+], \tag{13}$$

where $\hat{G}$ is the Green's function in the tight-binding representation, $^+$ stands for Hermitian conjugate, and $\hat{\Gamma}_{s/d}$ are the rate matrices of electron exchange with source and drain, $\hat{\Gamma}_{s/d} = i[\hat{\Sigma}_{s/d} - \hat{\Sigma}^+_{s/d}]$ [37]. The expression for transmission $\mathcal{T}_0$ is greatly simplified in 1D atomic chains, where $\hat{\Sigma}$-operators act only at the terminal sites [39]

$$\mathcal{T}_0(E) = 4\Im g_s(E)\Im g_d(E)|\langle 1|\hat{G}(E)|n_{\mathrm{at}}\rangle|^2; \tag{14}$$

here, $\Im$ stands for the imaginary part. In other words, the transmittance is proportional to the modulus squared of source-drain propagator $|\langle 1|\hat{G}|n_{\mathrm{at}}\rangle|^2$.

Our next goal is to modify the Eqs. (12) and (13) to account for electron-cavity interactions to an arbitrary order of the interaction strength. The first crucial building block in this modification is the system's density matrix," electron in the leads + cavity". We assume that the electromagnetic field does not penetrate the metal leads, and that the strong electron scattering quickly destroys the electron-photon coherence. This implies that electronic and photonic degrees of freedom are decoupled in the leads and obey the Gibbs distribution. Formally, the elements of the density matrix in the leads between the states $|\alpha\rangle = |i, N\rangle$ and $|\alpha'\rangle = |i', N'\rangle$ are given by

$$\langle\alpha'|\hat{\rho}|\alpha\rangle = \langle i'|\hat{\rho}_e|i\rangle \otimes \langle N'|\hat{\rho}_{ph}|N\rangle. \tag{15}$$

The ordinary Gibbs distribution gives the photonic part of the density matrix for N photons in the mode

$$\langle N'|\hat{\rho}_{ph}|N\rangle = \frac{1}{Z}\delta_{NN'}\exp(-N\hbar\omega/kT), \tag{16}$$

$Z = [1 - e^{-\beta\hbar\omega}]^{-1} \equiv n_B(\omega) + 1$ is the statistical sum for an individual cavity mode, where $n_B(\omega)$ is the Bose function of energy $\hbar\omega$. The electron density matrix obeys the Fermi distribution with energy ε and chemical potential μ:

$$\langle i'|\hat{\rho}_e|i\rangle = \int_{-\infty}^{+\infty} d\varepsilon A_{ii'}(\varepsilon)n_F(\varepsilon), \tag{17}$$

here $A_{ii'}(\varepsilon)$ is the electron's spectral function in the leads, and $n_F(\varepsilon) = [e^{(\varepsilon-\mu)/kT} + 1]^{-1}$ is the electron's Fermi function.

The absence of electron-cavity interactions in the leads enables us to introduce the well-defined occupation numbers for dressed electrons with given total energy E and photon number N:

$$n(E, N) = n_F(E - N\hbar\omega) \times \frac{e^{-N\hbar\omega/kT}}{n_B(\omega) + 1}. \tag{18}$$

Summation of $n(E, N)$ with respect to photon numbers N yields $n_F(\varepsilon)$, reflecting the problem's single-electron nature. The Landauer-like formula can now be written down for these

new noninteracting dressed electrons as (see Appendix B):

$$I = \frac{2e}{h}\sum_{N,M}\int dE[n_s(E,N) - n_d(E,M)]\mathcal{T}_{NM}(E), \quad (19)$$

where $n_{s/d}$ are the occupation numbers for the dressed electrons in the source and drain. In the Boltzmann limit, the occupation numbers $n(E,N)$ would depend only on total energy, $n(E,N) \approx e^{-(E-\mu)/kT}/[n_B(\omega)+1]$. The generalized Landauer formula becomes especially simple

$$I = \frac{2e/h}{n_B(\omega)+1}\int_{-\infty}^{+\infty} dE[f_s(E) - f_d(E)]\sum_{N,M=0}^{+\infty}\mathcal{T}_{NM}(E), \quad (20)$$

where $f_{s/d}(E) = e^{-(E-\mu_{s/d})/kT}$ is the Boltzmann exponent for the energy E. Above, $\mathcal{T}_{NM}(E)$ is the probability of electron transmission from the source with N photons in the cavity to the drain with M photons in the cavity. The expression for photon-number-resolved transmittance generalizes the results (13) and (14):

$$\begin{aligned}\mathcal{T}_{NM} &= \mathrm{Tr}[\langle N|\hat{\Gamma}_S|N\rangle\langle N|\hat{G}|M\rangle\langle M|\hat{\Gamma}_D|M\rangle\langle M|\hat{G}^+|N\rangle] \\ &= 4\Im g_s(E - N\hbar\omega)\Im g_d(E - M\hbar\omega)|\langle N,1|\hat{G}|n_{\mathrm{at}},M\rangle|^2.\end{aligned} \quad (21)$$

The diagonal elements $\mathcal{T}_{NN}$ show the probabilities of electron transfer between source and drain without real photon excitation. Yet, virtual photon emission along the path is fully included into $\mathcal{T}_{NN}$. The off-diagonal elements $\mathcal{T}_{NM}$ stand for probabilities of assisted tunneling, and $M-N$ is the number of emitted/absorbed real photons during a single electron passage.

The modified Landauer formula (20) is applicable only at low fermion occupation numbers $n_F \ll 1$. This corresponds to the Fermi levels μ_s and μ_d lying outside the conduction band. Thermally excited carriers carry the current in such a situation with $E > \{\mu_s, \mu_d\}$. Otherwise, the Pauli blocking principle would hinder the emission of cavity photons [32].

The practically measured quantity is the conductance $G = \partial I/\partial V_{SD}$. To single out the contributions of photon-assisted and elastic transport, we endow G with photon indices G_{NM} and define it according to

$$G_{NM} = \frac{G_Q}{n_B(\omega)+1}\int \mathcal{T}_{NM}(E)e^{\frac{E}{kT}}\frac{dE}{kT}. \quad (22)$$

The physical meaning of G_{NM} is the part of total conduction, where an electron enters the cavity with N photons and emits/absorbs $M-N$ photons during its path. Above, we have introduced $G_Q = [2e^2/h]e^{+\mu/kT}$, the conductance quantum timed by the Boltzmann distribution at the band edge, $\mu = (\mu_s+\mu_d)/2$. The Fermi level μ in the nondegenerate semiconductor affects the conductivity only via a multiplicative factor $e^{+\mu/kT} < 1$.

III. RESULTS: MODIFICATIONS OF ONE-DIMENSIONAL CONDUCTANCE DUE TO CAVITY COUPLING

We proceed to examine the effects of cavity coupling on the transmittance spectrum $\mathcal{T}(E)$ and thermally averaged conductance G in 1D atomic chains. These quantities were obtained via a numerical computation of Green's functions (7) and subsequent evaluation of transmittance (21) and conductance (22). The number of excited cavity states is chosen adaptively to ensure the convergence of transmission coefficient $\mathcal{T}_{00}$ with 1% accuracy. In the following calculations, such convergence required from 1 to 9 excited cavity states, depending on the coupling strength γ.

We begin the discussion of our numerical results by considering a relatively high photon energy, $\hbar\omega = 0.6\,\mathrm{eV}$, comparable to the bandwidth $4t = 1.6\,\mathrm{eV}$ and significantly exceeding the disorder amplitude $\delta U = 0.2\,\mathrm{eV}$. The chain length is $n_{\mathrm{at}} = 60$. The computed plots of transmittance spectra $\mathcal{T}_{00}(E)$ (ground-state transmittance) and $\mathcal{T}_{01}(E)$ (transmittance with an associated one-photon emission) are shown in Fig. 2(a). Figures 2(b)– 2(d) display the magnified views of the transmittance in several characteristic energy ranges. In the absence of cavity, $\mathcal{T}_{00}(E)$ exhibits several sharp resonances corresponding to the electron passage along the quasibound states E_i in the random potential. The transmittance envelope drops to zero at the lower and upper band edges due to the predominant localization of states with small group velocities.

The main effects of the cavity on transport consist in (1) the emergence of additional resonant structures in $\mathcal{T}_{00}(E)$ (2) the onset of electroluminescence $\mathcal{T}_{01}(E)$ at energies $E > \hbar\omega$. Each new resonant structure appears approximately at energies $E = E_i + \hbar\omega$. In other words, it represents a photon replica of an original resonant path. The two electron paths, one without photon emission and the other with photon emission and reabsorption, interfere with each other. This interference results in the appearance of a characteristic Fano structure in the original transmission curve $\mathcal{T}_{00}(E)$. The width and amplitude of the new Fano resonance depend on the position of the electron state E with respect to the midband.

In the high-energy sector, $E \lesssim 4t$, the Fano structures in the transmittance $\mathcal{T}_{00}$ are broad and faint. Simultaneously, the amplitude of electroluminescence $\mathcal{T}_{01}$ is relatively high and may exceed the zero-photon transmission at relatively small coupling [$\gamma^* \approx 10\,\mathrm{meV}$ in Fig. 2(d)]. In this situation, the zero-photon path $\mathcal{T}_{00}$ is suppressed due to the carrier localization at the upper band edge, and the original bound states are weakly coupled to the leads. After cavity photon emission, the electron energy gets closer to the midband, where both group velocity and coupling to the leads are more significant. These final states have relatively short lifetimes and decay quickly by releasing the electron to the leads. In such a situation, the electroluminescence process readily dominates the zero-photon transmission.

At intermediate energies, $E \sim 2t$, an original electron has a relatively large group velocity and is less prone to localization in a disorder potential. The emission of a virtual photon now pushes the electrons closer to the band bottom, i.e., to the states weakly coupled to the leads. The weak coupling of the final state to the leads results in a narrow Fano resonance in the original transmission curve $\mathcal{T}_{00}(E)$ [Fig. 2(c)]. The coupling of the final state to the leads also results in an electroluminescence peak, albeit weaker than in the high-energy sector.

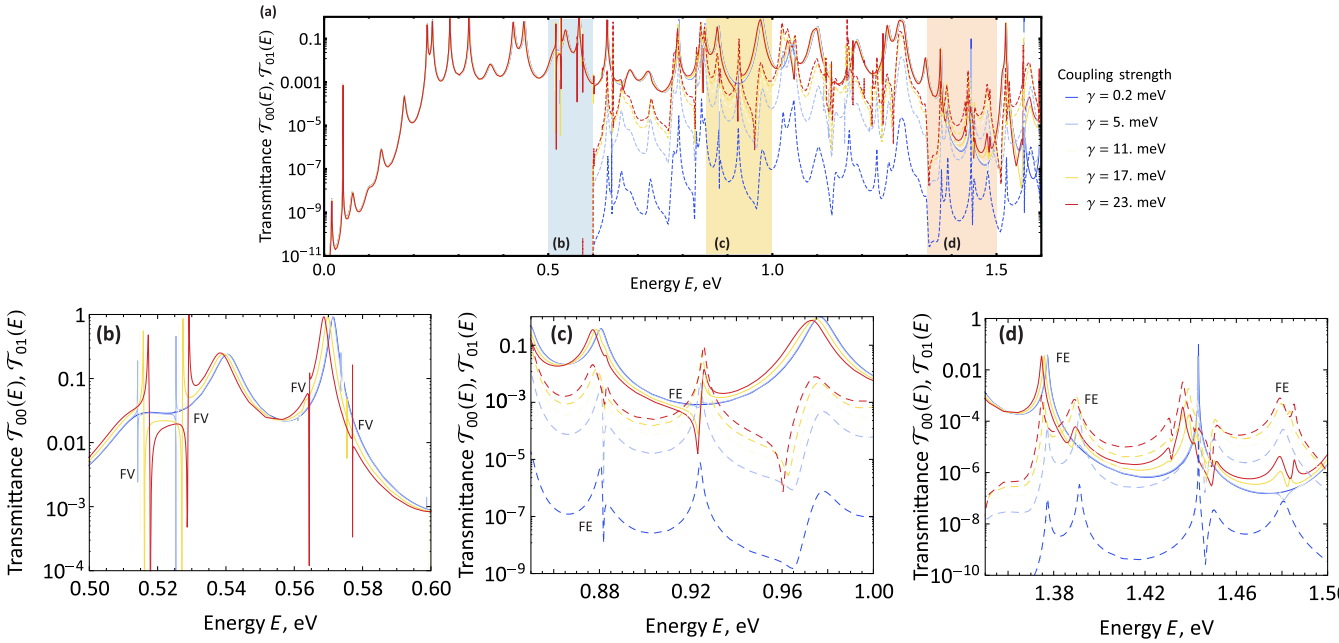

FIG. 2. Effect of the cavity on the electron transmission through a disordered 1D chain. (a) Energy-dependent transmission coefficients without real photon emission $\mathcal{T}_{00}$ (solid) and with single real photon emission $\mathcal{T}_{01}$ (dashed). The coupling strength varies from 0.2 to 23 meV; photon energy is $\hbar\omega = 0.6\,\text{eV}$, and the disorder amplitude is $\delta U = 0.2\,\text{eV}$, disorder realization corresponds to sample No.2*S* described in the Supplemental Material [40] (b)(–d) Magnified views of transmittance in selected energy sectors. (b) In the low-energy region $E < \hbar\omega$, an electron can emit a virtual photon and travel along a bound state in the disorder potential. This results in Fano interference of the original path and path with virtual photon emission (denoted as FV). (c) At intermediate energies, $E \gtrsim \hbar\omega$, the emission of a cavity photon moves the electron to a quasi-bound state weakly coupled to the leads, leading to a broad Fano resonance and the appearance of electroluminescence (denoted as FE). (d) At high energies, $E \sim 4t$, the emission of a cavity photon propels the electron into the state, rapidly decaying to the leads, resulting in the dominance of electroluminescence.

At even lower energies $E < \hbar\omega$, an electron is incapable of real photon emission. Nevertheless, its transmission curve $\mathcal{T}_{00}(E)$ acquires extra Fano resonant structures due to the emission of virtual photons [FV-peaks in Fig. 2(b)]. The disordered character of the potential enables the very possibility of these low-energy peaks. A disordered *noninteracting* chain has several energy levels truly bound in the random potential with energies $E_i < 0$. An electron incident on the *interacting chain* can gain access to these levels via emission and reabsorption of the virtual cavity photons [process No. (1) in Fig. 1(a)]. The linewidth of these Fano-type structures is proportional to the virtual photon emission and re-absorption probability, $\Gamma \sim \gamma^2/\omega$, and is thus very small.

Exploring cavity effects on electron transmission $\mathcal{T}(E)$ across a wide energy range is primarily of academic interest. Indeed, all electron states relevant to transport in nondegenerate semiconductors are located at energies $E \sim kT$ from the lower band edge. Consequently, only modifications to the low-energy transmittance $\mathcal{T}(E)$ can influence the thermally-averaged conductance $G(T)$.

To investigate modifications in transmittance pertinent to the conductivity of nondegenerate semiconductors, we concentrate on the low-energy sector of the simulated $\mathcal{T}_{00}(E)$. Initially, we maintain the same photon energy, $\hbar\omega = 0.6\,\text{eV}$, and present the results in Figs. 3(a) and 3(b). The first effect of the cavity in this sector is manifested by a slight *upward* spectral shift of the transmission resonances. The sign of the shift may seem unusual because the second-order perturbative correction to the energy of the ground state expressed as

$$\delta^{(1)}E_i = e^2 \sum_k \frac{|X_{ik}|^2 |\mathcal{E}_{\text{vac}}|^2}{E_i - (E_k + \hbar\omega)} \tag{23}$$

should always be negative (here X_{ik} is the matrix element of the electron coordinate and $\mathcal{E}_{\text{vac}} = i\omega A_{\text{vac}}/c$ is the zero-point electric field). The explanation of the positive shift lies in the two facts. First, the lowest resonance in $\mathcal{T}_{00}(E)$ does not necessarily correspond to the lowest energy level of the interacting chain. As discussed above, even lower levels bound in the random potential are present at $E < 0$. The interaction of the lowest resonance with these levels may lead to positive energy shifts.

Second, another diamagnetic correction exists apart from the virtual photon correction to the energies given by Eq. (23). It is also quadratic in the electron-photon coupling and appears in the first order of the perturbation theory:

$$\delta^{(2)}E_i = \frac{e^2}{2mc^2} A_{\text{vac}}^2 = 2\frac{\gamma^2}{t}. \tag{24}$$

As a result of the two perturbations mentioned above, most resonances in $\mathcal{T}(E)$ in the low-energy sector for disordered chains are generally shifted upwards in energy with increasing the cavity coupling γ. This reduces the thermally averaged conductance at low temperatures as the coupling strength γ is increased. This range of temperatures and coupling strengths is highlighted in Fig. 3(b) with a dashed rectangle.

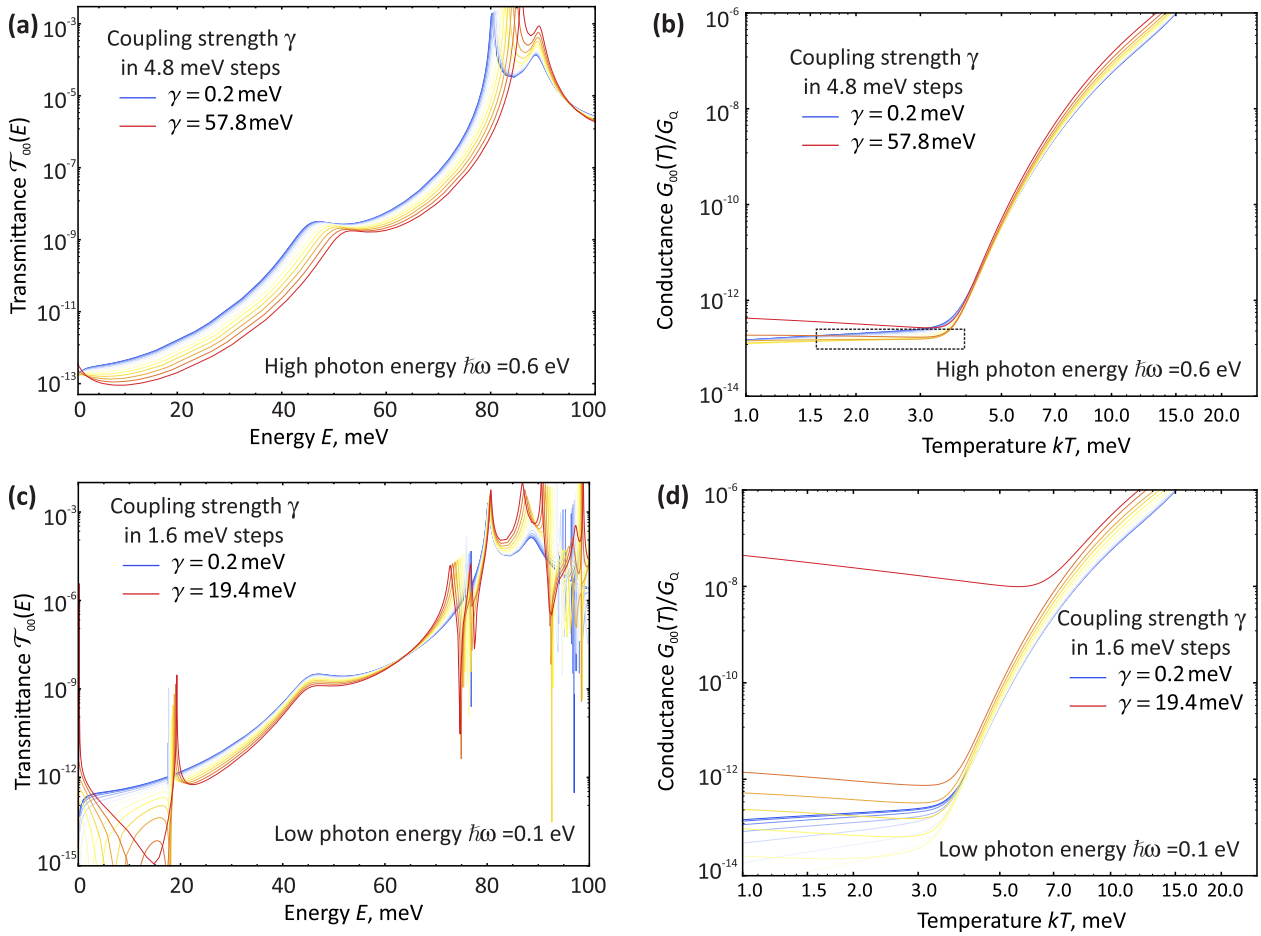

FIG. 3. Cavity-induced changes in energy-resolved transmittance and thermally averaged conductance. The results are obtained for an atomic chain with $n_{\rm at} = 60$, disorder amplitude $\delta U = 0.2\,$eV, bandwidth $4t = 1.6\,$eV, disorder realization corresponds to sample No.1S described in the Supplemental Material [40]. (a), (b) Simulation for a photon energy $\hbar\omega = 0.6\,$eV larger than the disorder amplitude. (c), (d) The same disorder realization for photon energy $\hbar\omega = 0.1\,$eV, smaller than the disorder amplitude. The teft and right columns display the transmittance spectra and the corresponding thermally-averaged conductance.

The second effect of cavity coupling is also related to positive energy shifts of levels with increasing the coupling strength γ. It lies in rising energy levels from the band of strictly localized states $E < 0$ to the band of accessible energies $E > 0$. More precisely, a discrete level in the disorder potential with a low binding energy $-|E_b|$ may acquire a positive correction (24). Its net final energy $-|E_b| + \delta^{(1)}E + \delta^{(2)}E > 0$ thus becomes accessible to the carriers incident from the leads. Such a prolumination of the energy levels by cavity results in the emergence of a resonance in transmission $\mathcal{T}_{00}(E)$ at nearly zero energy [see the red curve in Fig. 3(a) in the vicinity of $E \approx 0$]. The low-energy resonance, in turn, implies a positive correction to the conductance at low temperatures, $\partial G/\partial\gamma|_{T\to 0} > 0$. While the low-temperature conductance is enhanced via coupling to the cavity, the temperature dependence of conductance becomes anomalously decaying, $\partial G/\partial T < 0$, see the negative slope of the red curve in Fig. 3(b). The latter effect stems from an abrupt decrease in $\mathcal{T}_{00}(E)$ with energy at the right shoulder of the transmission resonance.

The modification of conductance associated with the prolumination of the weakly bound states is more pronounced with decreasing the cavity photon energy. This is best illustrated in Figs. 3(c)–3(d), where the same disorder realization is studied at cavity photon energy $\hbar\omega = 0.1$. The zero-energy resonance in transmission becomes visible already at coupling strength $\gamma^* \sim 10\,$meV, which is six times smaller than the corresponding γ^* at high photon energy $\hbar\omega = 0.6\,$eV. The reason for more substantial cavity effects at low photon energies lies in smaller energy denominators in Eq. (23), and thus in larger perturbative energy shifts at a fixed value of γ [41]. Increasing γ to even higher values shifts the resonance away from $E \approx 0$, reducing the conduction.

Another set of modifications in $\mathcal{T}_{00}(E)$ at the band bottom is associated with the emergence of sharp Fano resonances. An electron at nearly zero energy $E \approx 0$ can emit the virtual photon and jump to a discrete level in the disorder potential. The sharp Fano structure discussed above can now appear at the lower band edge, as illustrated in Fig. 3(c). Though the Fano structures modify the transmission spectra, their effect on the T-dependent conductance is nonunivocal. Indeed, a sharp increase in $\mathcal{T}_{00}(E)$ in a narrow range of energies can be compensated by a transmission drop at other energies. Further examples of cavity modifications of conductance for various disorder realizations can be found in the Supplemental Material [40].

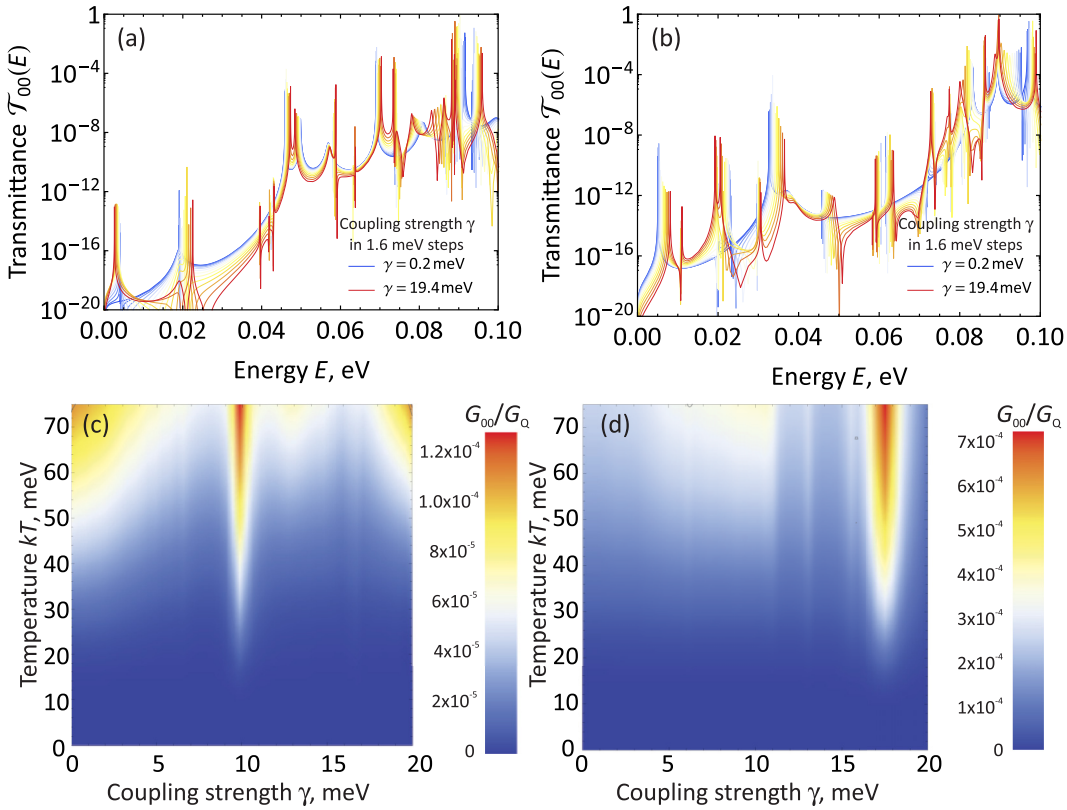

FIG. 4. Effect of cavity on 1D localization in long conductors. Simulated energy-resolved transmittance $\mathcal{T}_{00}(E)$ (top row) and thermally averaged conductance $G_{00}(T, \gamma)$ for chain length $n_{at} = 120$, photon energy $\hbar\omega = 0.1$ eV, disorder amplitude $\delta U = 0.2$ eV. (a) and (c) correspond to sample #3L, while (b) and (d) correspond to sample #4L (described in detail in the Supplemental Material). The conductance generally reaches a maximum at some γ corresponding to the passage of the bound state through the conduction band bottom.

Most cavity effects on conductance seen in the vicinity of the band bottom are associated with the presence of bound states in the disordered potential. It is natural to assume that an increase in the chain length, at the same disorder statistics, would enhance the number of bound levels. As soon as the electron's motion remains coherent throughout the chain, longer chains should be more susceptible to cavity effects. This suggestion is fully confirmed in Fig. 4, where we present the transmission simulations for a chain of length $n_{at} = 120$, twice longer than that in Figs. 2 and 3, and at four different realizations of disorder. The number of transmission resonances (ordinary and Fano-type) per unit energy window is much bigger than that for short chains. A weakly bound state crosses the band bottom $E = 0$ for most disorder realizations as the coupling constant increases. This effect results in non-monotonic γ dependence of the thermally averaged conductance.

IV. DISCUSSION OF THE RESULTS

We have uncovered several effects of electron-photon coupling leading to conductivity modification in the localized regime for non-degenerate carrier statistics. The first class of changes is associated with Fano resonances in transmission, which are associated with the emission of virtual cavity photons and the passage of electrons along the bound levels in the disorder potential. This effect is observable only at small photon energies compared to the disorder amplitude $\hbar\omega \lesssim \delta U$. Another prerequisite for this effect is the absence of degeneracy within the bound states, i.e., that $|\mu - E_c| > \delta U$. Otherwise, Pauli blocking strongly constrains both real and virtual photon emission processes.

The second class of cavity effects on the 1D conductivity involves potentially significant shifts in bound and quasibound energy levels as the coupling strength increases. The cavity-induced diamagnetic correction to the energy levels is always positive, while the sign of the virtual-photon correction remains indeterminate. These energy shifts induced by the cavity are most notable for conduction when an initially bound state transitions to a quasibound state, becoming accessible to electrons incident from the leads. Such an energy shift implies cavity-enhanced conduction at low temperatures. The observation of this effect necessitates a well-defined conduction band edge in the leads; otherwise, there would be no clear boundary between bound and quasibound states.

Although our discussion has been confined to 1D systems, we expect the aforementioned cavity effects to be generic and applicable to 2D and 3D systems. The impact of the cavity on energy levels in 2D systems is expected to be particularly pronounced, given that the binding energy in disordered 2D systems is exponentially small. Consequently, placing disordered 2D systems in cavities should lead to the delocalization of weakly bound states, enabling their contribution to transport.

Finally, we estimate whether the coupling constant $\gamma \sim 0.1$ meV, for which we observe the cavity effects on the conductance in Figs. 3 and 4, is realistic. By relating γ to cavity parameters and assuming the cavity has volume V, we obtain the expression

$$\gamma = \left(\frac{e^2}{\hbar c}\right)^{1/2} \frac{\hbar^2}{2m^* a}\left(\frac{\lambda}{V}\right)^{1/2}, \tag{25}$$

where we have introduced the effective mass according to $t = \hbar^2/2m^*a^2$. Taking the minimum possible mode volume $V = \lambda^3$, we simplify Eq. (25) to

$$\gamma = \left(\frac{e^2}{\hbar c}\right)^{1/2} \frac{\hbar^2}{2m^* a\lambda}. \tag{26}$$

The numerical estimate for $m^* = 0.067m_0$ (GaAs quantum wire), $a = 0.5$ nm and $\lambda = 10$ μm provides $\gamma = 0.1$ meV. Fortunately, this corresponds to pronounced cavity effects on conduction at the lower band edge. Higher values of γ may be achievable in 2D plasmonic cavities [42]. The characteristic wavelength of 2D plasmons is $\sim 10^2$ times below the free-space photon wavelength. With this compression ratio, 2D plasmonic cavities can provide $\sim 10^3$-fold enhancement of the coupling constant. Another approach toward increasing the coupling strength is placing 1D conductors into the cavities with field singularities near metallic edges. The most prominent example of such a cavity is a slot in a planar metallic pad [18,19]. Although the average amplitude of fluctuations in such cavity is still given by $A_{\rm vac} = (2\pi\hbar c/\omega V)^{1/2}$, the local values of the field near the slot edges can reach much higher values.

The temperature-dependent conduction of 1D chains in a cavity $G(T, \gamma)$ can strongly differ from the respective quantity in the uncoupled structure, $G(T, \gamma = 0)$. However, the temperature dependence $G(T)$ in an interacting chain does not exhibit any distinctive features not already present at $\gamma = 0$. Conduction measurements at variable coupling strength are necessary to reveal the effect of coupling. Fortunately, corresponding setups based on movable Bragg mirrors are available [43,44].

ACKNOWLEDGMENTS

The work of D.S. and G.A. was supported by the 22-29-01034 grant from the Russian Science Foundation. L.M.-M. acknowledges Project No. PID2020-115221GB-C41, financed by MCIN/AEI/10.13039/501100011033 and the Aragon Government through Project Q-MAD. The authors thank V. Vyurkov and V. Muravev for fruitful discussions.

APPENDIX A: NUMERICAL REALIZATION OF ELECTRON-CAVITY HAMILTONIAN

For computational purposes, obtaining the representation of the Hamiltonians in the matrix form is necessary. Below, we establish the structure of the respective matrices. The photon and electron degrees of freedom are coupled in the interacting channel. The dressed electron states in the channel are characterized by their position in the chain and number of cavity photons. In the tight-binding representation for electronic degrees, and occupation-number representation for photonic degrees, this is a vector of length $N_{ph} \times n_{\rm at}$, where $n_{\rm at}$ is the number of atomic sites and N_{ph} is the number of photonic states. The latter is retained finite in numerical calculations. The size of corresponding Hamiltonian matrix is $(N_{ph} \times n_{\rm at}) \times (N_{ph} \times n_{\rm at})$. In all our numerical calculations, we arrange the Hamiltonian matrices in the block form

$$\hat{\mathcal{H}} = \begin{pmatrix} \langle 0|\hat{\mathcal{H}}|0\rangle & \langle 0|\hat{\mathcal{H}}|1\rangle & \langle 0|\hat{\mathcal{H}}|2\rangle & \dots \\ \langle 1|\hat{\mathcal{H}}|0\rangle & \langle 1|\hat{\mathcal{H}}|1\rangle & \langle 1|\hat{\mathcal{H}}|2\rangle & \dots \\ \langle 2|\hat{\mathcal{H}}|0\rangle & \langle 2|\hat{\mathcal{H}}|1\rangle & \langle 2|\hat{\mathcal{H}}|2\rangle & \dots \\ \dots & \dots & \dots & \dots \end{pmatrix}, \tag{A1}$$

where brackets $\langle N|\hat{\mathcal{H}}|N'\rangle$ stand for taking the matrix elements between Nth and N'th states of electromagnetic field. Each element of the block matrix above is the matrix of size $n_{\rm at} \times n_{\rm at}$; it acts already in the tight-binding subspace.

Below, we present the block representation of operators constituting $\hat{\mathcal{H}}$. The field term is diagonal,

$$\langle N|\hat{\mathcal{H}}_f|N'\rangle = \hat{I}\delta_{NN'}N\hbar\omega, \tag{A2}$$

where the identity operator $\hat{I}$ acts in the tight-binding space.

The tight-binding diagonal and tight-binding off-diagonal matrix elements of chain Hamiltonian are different. The diagonal elements are simply the on-site energies. The off-diagonal elements are the hopping energies modified by electromagnetic fluctuations. Collected together, they form the matrices

$$\langle N|\hat{\mathcal{H}}_{\rm ch}(\gamma)|N'\rangle = \delta_{NN'}\begin{pmatrix} U_1 & 0 & 0 & 0 & \dots \\ 0 & U_2 & 0 & 0 & \dots \\ 0 & 0 & U_3 & 0 & \dots \\ \dots & \dots & \dots & \dots & \dots \\ \dots & 0 & 0 & 0 & U_{n_{\rm at}} \end{pmatrix} + t\begin{pmatrix} 0 & h_{NN'}\left(\frac{\gamma}{t}\right) & 0 & 0 & \dots \\ h_{NN'}\left(-\frac{\gamma}{t}\right) & 0 & h_{NN'}\left(\frac{\gamma}{t}\right) & 0 & \dots \\ 0 & h_{NN'}\left(-\frac{\gamma}{t}\right) & 0 & h_{NN'}\left(\frac{\gamma}{t}\right) & \dots \\ \dots & \dots & \dots & \dots & \dots \\ \dots & 0 & 0 & h_{NN'}\left(-\frac{\gamma}{t}\right) & 0 \end{pmatrix}. \tag{A3}$$

Above, we have introduced an auxiliary function

$$h_{NM}(g) = \langle N|\exp(-ig[\hat{b} + \hat{b}^+])|M\rangle, \tag{A4}$$

which is the matrix elements of harmonic exponent between Nth and Mth states of the oscillator, $g = \gamma/t$. Explicit calcu-

lation of h_{NM} factors is done with Baker-Campbell-Hausdorff formula:

$$\exp(-ig[\hat{b}+\hat{b}^+]) = e^{-g^2/2}\exp(-ig\hat{b}^+)\exp(-ig\hat{b}). \quad \text{(A5)}$$

The exponent of annihilation operator $\exp(-ig\hat{b})|M\rangle$ produces only finite sums. Expanding the exponent in a Taylor series can evaluate them in closed form. This results in

$$h_{NM}(g) = \langle N|\exp(-ig[\hat{b}+\hat{b}^+])|M\rangle = e^{-g^2/2}\sum_{s=0}^{N}\sum_{j=0}^{M}\frac{(ig)^s}{s!}\frac{(ig)^j}{j!}\delta_{N-s,M-j}P(j,M)P(s,N), \quad \text{(A6)}$$

$$P(j,M) = \sqrt{[M-(j-1)][M-(j-2)]...[M-1]M}. \quad \text{(A7)}$$

For example, some of the lowest elements are

$$h_{00}(g) = e^{-g^2/2}, \quad h_{11}(g) = e^{-g^2/2}(1-g^2),$$
$$h_{01}(g) = ige^{-g^2/2}, \quad h_{02}(g) = -\frac{1}{\sqrt{2}}g^2e^{-g^2/2}. \quad \text{(A8)}$$

APPENDIX B: PHOTON-DRESSED ELECTRONS AND THE GENERALIZED LANDAUER FORMULA

The usual Landauer's formula is derived for noninteracting electrons. Therefore, we must cast the Hamiltonian (4) into a noninteracting form. We introduce auxiliary creation/annihilation operators $\hat{c}_{iN}$, $\hat{c}_{iN}^+$ describing a fictitious fermion on a 2D lattice. Electron and photon creation/annihilation operators can be written as

$$\hat{a}_i^+\hat{a}_j = \sum_{N=0}^{\infty}\hat{c}_{iN}^+\hat{c}_{jN}, \quad \text{(B1)}$$

$$\hat{b} = \sum_{i=1}^{n_{\rm at}}\sum_{N=0}^{\infty}\sqrt{N+1}\hat{c}_{iN}^+\hat{c}_{i,N+1}. \quad \text{(B2)}$$

Since only one $|iN\rangle$ state can be occupied, quartic terms in the Hamiltonian will reduce to the quadratic ones:

$$\hat{c}_1^+\hat{c}_2\hat{c}_3^+\hat{c}_4 = \hat{c}_1^+\hat{c}_4\delta_{23} - \hat{c}_1^+\hat{c}_3^+\hat{c}_2\hat{c}_4 = \hat{c}_1^+\hat{c}_4\delta_{23}. \quad \text{(B3)}$$

Therefore,

$$\left(\sum_{j=1}^{n_{\rm at}}\sum_{N=0}^{\infty}\sqrt{N+1}\hat{c}_{jN}^+\hat{c}_{j,N+1}\right)^k = \sum_{j=1}^{n_{\rm at}}\sum_{N=0}^{\infty}\sqrt{\frac{(N+k)!}{N!}}\hat{c}_{jN}^+\hat{c}_{j,N+k}, \quad \text{(B4)}$$

$$\exp\left(\alpha\sum_{j=1}^{n_{\rm at}}\sum_{N=0}^{\infty}\sqrt{N+1}\hat{c}_{jN}^+\hat{c}_{j,N+1}\right) = \sum_{k=0}^{\infty}\sum_{j=1}^{n_{\rm at}}\sum_{N=0}^{\infty}\frac{\alpha^k}{k!}\sqrt{\frac{(N+k)!}{N!}}\hat{c}_{jN}^+\hat{c}_{j,N+k}, \quad \text{(B5)}$$

$$e^{\pm\frac{i\gamma}{t}(\hat{b}+\hat{b}^+)} = e^{-\frac{1}{2}\left(\frac{\gamma}{t}\right)^2}e^{\pm\frac{i\gamma}{t}\hat{b}^+}e^{\pm\frac{i\gamma}{t}\hat{b}} = e^{-\frac{1}{2}\left(\frac{\gamma}{t}\right)^2}\left[\exp\left(\mp\frac{i\gamma}{t}\sum_{j=1}^{n_{\rm at}}\sum_{N=0}^{\infty}\sqrt{N+1}\hat{c}_{iN}^+\hat{c}_{i,N+1}\right)\right]^+\exp\left(\pm\frac{i\gamma}{t}\sum_{j=1}^{n_{\rm at}}\sum_{N=0}^{\infty}\sqrt{N+1}\hat{c}_{iN}^+\hat{c}_{i,N+1}\right)$$
$$= e^{-\frac{1}{2}\left(\frac{\gamma}{t}\right)^2}\sum_{j=1}^{n_{\rm at}}\sum_{k,M,N=0}^{\infty}\frac{k!}{\sqrt{M!N!}}\binom{M}{k}\binom{N}{k}\left(\pm\frac{i\gamma}{t}\right)^{M+N-2k}\hat{c}_{jM}^+\hat{c}_{jN}.$$

Now, we can rewrite the system's Hamiltonian as

$$\hat{H} = \hbar\omega\hat{b}^+\hat{b} + \sum_{i=1}^{n_{\rm at}}U_i\hat{a}_i^+\hat{a}_i + \sum_{\pm}\sum_{i=1}^{n_{\rm at}}te^{\pm\frac{i\gamma}{t}(\hat{b}+\hat{b}^+)}\hat{a}_{i\pm1}^+\hat{a}_i = \sum_{i=1}^{n_{\rm at}}\sum_{N=0}^{\infty}(U_i+N\hbar\omega)\hat{c}_{iN}^+\hat{c}_{iN}$$
$$+\sum_{\pm}\sum_{i=1}^{n_{\rm at}}te^{-\frac{1}{2}\left(\frac{\gamma}{t}\right)^2}\sum_{k,M,N=0}^{\infty}\frac{k!}{\sqrt{M!N!}}\binom{M}{k}\binom{N}{k}\left(\pm\frac{i\gamma}{t}\right)^{M+N-2k}\hat{c}_{i\pm1,M}^+\hat{c}_{iN}, \quad \text{(B6)}$$

and similarly for the lead terms. What is important is that the Hamiltonian now has the same form as for noninteracting electrons,

$$\hat{H} = \sum_{ijMN}h_{iMjN}\hat{c}_{iM}^+\hat{c}_{jN}. \quad \text{(B7)}$$

We can also rewrite the charge density operator:

$$\rho_i = -e\hat{a}_i^+\hat{a}_i = -e\sum_{N=0}^{\infty}\hat{c}_{iN}^+\hat{c}_{iN}. \quad \text{(B8)}$$

The current density operator can be deduced from the continuity equation.

Now, it is obvious that the electric current can be calculated via the usual Landauer-Buttiker formula applied to the 2D lattice described by Hamiltonian (B6):

$$I = \sum_{N_s}J_{N_d} = \sum_{N_s,N_d}\frac{e}{h}\int dE[n_s(E;N_s) - n_d(E;N_d)]T_{N_sN_d}(E),$$

where E is the energy of the dressed fermion described by Hamiltonian (B6).

In this derivation, we initially assume the presence of a single electron in the system, allowing us to neglect electron-electron interactions. Now, we extend our analysis to the case of multiple electrons while still disregarding electron-electron

interactions. The total current in this scenario results from the sum of currents carried by each photon-dressed electron following the Hamiltonian (B6). While the expression (B9) remains unaltered, it is important to note that the occupation numbers no longer need to sum up to unity.

As electrons in the leads do not interact with photons, we can express the occupation numbers in the leads as products of electronic and photonic occupation numbers:

$$n_{s/d}(E;N_{s/d}) = n_{F\,s/d}(\varepsilon)\frac{e^{-\frac{N_{s/d}\hbar\omega}{kT}}}{1+e^{-\frac{\hbar\omega}{kT}}+e^{-\frac{2\hbar\omega}{kT}}+\cdots} = n_{F\,s/d}(E-N_{s/d}\hbar\omega)\frac{e^{-\frac{N_{s/d}\hbar\omega}{kT}}}{n_B(\hbar\omega)+1}, \quad \text{(B9)}$$

and get

$$I = \frac{2e}{h}\frac{1}{n_B(\hbar\omega)+1}\sum_{N_s,N_d}\int dE \times \left[n_{F\,s}(E-N_s\hbar\omega)e^{-\frac{N_s\hbar\omega}{kT}} - n_{F\,d}(E-N_d\hbar\omega)e^{-\frac{N_d\hbar\omega}{kT}}\right] \times T_{N_sN_d}(E). \quad \text{(B10)}$$

Since the preceding derivation is meaningful only in the absence of degeneracy, one may substitute the Fermi distribution with its Boltzmann tail:

$$n_{F\,s}(E-N_s\hbar\omega)e^{-\frac{N_s\hbar\omega}{kT}} \approx \exp\left\{-\frac{E-N_s\hbar\omega-\mu_s}{kT}-\frac{N_s\hbar\omega}{kT}\right\} = \exp\left\{-\frac{E-\mu_s}{kT}\right\} \equiv f_s(E). \quad \text{(B11)}$$

As a result, the occupation numbers in the modified Landauer formula become the Boltzmann exponents of the total energy E, $f_{s/d}(E)$.

It is possible to demonstrate that the modified Landauer-type formula reduces to its original version (12) in the absence of electron-cavity coupling. In this limit, the photon number remains unchanged during the electron passage, which can be formally expressed as $\mathcal{T}_{NM} = \delta_{NM}\mathcal{T}_{NN}$. Moreover, the tunneling probability depends solely on the electron energy $\varepsilon = E - N\hbar\omega$ and not on the state of the cavity. Formally, this is represented by $\mathcal{T}_{NN}(E) = \mathcal{T}_{00}(E - N\hbar\omega)$. Shifting the variable of energy integration in each Nth term of the sum according to $\varepsilon = E - N\hbar\omega$ produces an extra multiplicative factor $f(E) = e^{-N\hbar\omega/kT}f(\varepsilon)$. Summing up these multiplicative factors $\sum N = 0^{\infty}e^{-N\hbar\omega/kT} = n_B(\omega)+1$, we realize that all the information about the state of the cavity contained in the $n_B(\omega)$ functions has dropped out, leaving us with the original Landauer formula (12).

[1] J. Schwinger, On quantum-electrodynamics and the magnetic moment of the electron, Phys. Rev. **73**, 416 (1948).

[2] W. E. Lamb and R. C. Retherford, Fine structure of the hydrogen atom by a microwave method, Phys. Rev. **72**, 241 (1947).

[3] H. B. G. Casimir and D. Polder, The influence of retardation on the London-van der Waals forces, Phys. Rev. **73**, 360 (1948).

[4] P. Forn-Díaz, L. Lamata, E. Rico, J. Kono, and E. Solano, Ultrastrong coupling regimes of light-matter interaction, Rev. Mod. Phys. **91**, 025005 (2019).

[5] D. A. Iranzo, S. Nanot, E. J. C. Dias, I. Epstein, C. Peng, D. K. Efetov, M. B. Lundeberg, R. Parret, J. Osmond, J. Y. Hong, J. Kong, D. R. Englund, N. M. R. Peres, and F. H. L. Koppens, Probing the ultimate plasmon confinement limits with a van der Waals heterostructure, Science **360**, 291 (2018).

[6] Z. Shi, X. Hong, H. A Bechtel, B. Zeng, M. C Martin, K. Watanabe, T. Taniguchi, Y.-R. Shen, and F. Wang, Observation of a Luttinger-liquid plasmon in metallic single-walled carbon nanotubes, Nat. Photon. **9**, 515 (2015).

[7] Y. Ashida, A. İmamoğlu, J. Faist, D. Jaksch, A. Cavalleri, and E. Demler, Quantum electrodynamic control of matter: Cavity-enhanced ferroelectric phase transition, Phys. Rev. X **10**, 041027 (2020).

[8] M. A. Sentef, M. Ruggenthaler, and A. Rubio, Cavity quantum-electrodynamical polaritonically enhanced electron-phonon coupling and its influence on superconductivity, Sci. Adv. **4**, eaau6969 (2018).

[9] J. B. Curtis, Z. M. Raines, A. A. Allocca, M. Hafezi, and V. M. Galitski, Cavity quantum Eliashberg enhancement of superconductivity, Phys. Rev. Lett. **122**, 167002 (2019).

[10] M. Kiffner, J. R. Coulthard, F. Schlawin, A. Ardavan, and D. Jaksch, Manipulating quantum materials with quantum light, Phys. Rev. B **99**, 085116 (2019).

[11] O. V. Kibis, O. Kyriienko, and I. A. Shelykh, Band gap in graphene induced by vacuum fluctuations, Phys. Rev. B **84**, 195413 (2011).

[12] J. Román-Roche, F. Luis, and D. Zueco, Photon condensation and enhanced magnetism in cavity QED, Phys. Rev. Lett. **127**, 167201 (2021).

[13] G. M. Andolina, A. De Pasquale, F. M. D. Pellegrino, I. Torre, F. H. L. Koppens, and M. Polini, Can deep sub-wavelength cavities induce amperean superconductivity in a 2D material? arXiv:2210.10371.

[14] A. Thomas, E. Devaux, K. Nagarajan, T. Chervy, M. Seidel, D. Hagenmüller, S. Schütz, J. Schachenmayer, C. Genet, G. Pupillo *et al.*, Exploring superconductivity under strong coupling with the vacuum electromagnetic field, arXiv:1911.01459.

[15] A. Thomas, L. Lethuillier-Karl, K. Nagarajan, R. M. A. Vergauwe, J. George, T. Chervy, A. Shalabney, E. Devaux, C. Genet, J. Moran, and T. W. Ebbesen, Tilting a ground-state reactivity landscape by vibrational strong coupling, Science **363**, 615 (2019).

[16] B. Limbacher, M. A. Kainz, S. Schoenhuber, M. Wenclawiak, C. Derntl, A. M. Andrews, H. Detz, G. Strasser, A. Schwaighofer, B. Lendl, J. Darmo, and K. Unterrainer, Resonant tunneling diodes strongly coupled to the cavity field, Appl. Phys. Lett. **116**, 221101 (2020).

[17] E. Orgiu, J. George, J. A. Hutchison, E. Devaux, J. F. Dayen, B. Doudin, F. Stellacci, C. Genet, J. Schachenmayer, C. Genes, G. Pupillo, P. Samorì, and T. W. Ebbesen, Conductivity in organic semiconductors hybridized with the vacuum field, Nat. Mater. **14**, 1123 (2015).

[18] G. L. Paravicini-Bagliani, F. Appugliese, E. Richter, F. Valmorra, J. Keller, M. Beck, N. Bartolo, C. Rössler, T. Ihn,

K. Ensslin, C. Ciuti, G. Scalari, and J. Faist, Magneto-transport controlled by Landau polariton states, Nat. Phys. **15**, 186 (2019).

[19] F. Appugliese, J. Enkner, G. L. Paravicini-Bagliani, M. Beck, C. Reichl, W. Wegscheider, G. Scalari, C. Ciuti, and J. Faist, Breakdown of topological protection by cavity vacuum fields in the integer quantum Hall effect, Science **375**, 1030 (2022).

[20] F. Pisani, D. Gacemi, A. Vasanelli, L. Li, A. G. Davies, E. Linfield, C. Sirtori, and Y. Todorov, Electronic transport driven by collective light-matter coupled states in a quantum device, Nat. Commun. **14**, 3914 (2023).

[21] P. W. Anderson, D. J. Thouless, E. Abrahams, and D. S. Fisher, New method for a scaling theory of localization, Phys. Rev. B **22**, 3519 (1980).

[22] O. N. Dorokhov, Electron localization in a multichannel conductor, Zh. Eksp. Teor. Fiz. **85**, 1040 (1983) [Sov. J. Exp. Theor. Phys. **58**, 606 (1983)].

[23] N. Bartolo and C. Ciuti, Vacuum-dressed cavity magnetotransport of a two-dimensional electron gas, Phys. Rev. B **98**, 205301 (2018).

[24] M. Cirio, S. D. Liberato, N. Lambert, and F. Nori, Ground state electroluminescence, Phys. Rev. Lett. **116**, 113601 (2016).

[25] D. Hagenmüller, S. Schütz, J. Schachenmayer, C. Genes, and G. Pupillo, Cavity-assisted mesoscopic transport of fermions: Coherent and dissipative dynamics, Phys. Rev. B **97**, 205303 (2018).

[26] D. Hagenmüller, J. Schachenmayer, S. Schütz, C. Genes, and G. Pupillo, Cavity-enhanced transport of charge, Phys. Rev. Lett. **119**, 223601 (2017).

[27] C. J. Eckhardt, G. Passetti, M. Othman, C. Karrasch, F. Cavaliere, M. A. Sentef, and D. M. Kennes, Quantum floquet engineering with an exactly solvable tight-binding chain in a cavity, Commun. Phys. **5**, 122 (2022).

[28] C. F. Destefani, M. Villani, X. Cartoixà, M. Feiginov, and X. Oriols, Resonant tunneling diodes in semiconductor microcavities: Modeling polaritonic features in the terahertz displacement current, Phys. Rev. B **106**, 205306 (2022).

[29] D. A. Zezyulin, S. A. Kolodny, O. V. Kibis, I. V. Tokatly, and I. V. Iorsh, Dynamical stabilization by vacuum fluctuations in a cavity: Resonant electron scattering in the ultrastrong light-matter coupling regime, Phys. Rev. A **106**, 043708 (2022).

[30] V. V. Flambaum and V. G. Zelevinsky, Radiation corrections increase tunneling probability, Phys. Rev. Lett. **83**, 3108 (1999).

[31] R.-C. Ge, S. R. Koshkaki, and M. H. Kolodrubetz, Cavity induced many-body localization, arXiv:2208.06898.

[32] G. Arwas and C. Ciuti, Quantum electron transport controlled by cavity vacuum fields, Phys. Rev. B **107**, 045425 (2023).

[33] C. Ciuti, Cavity-mediated electron hopping in disordered quantum Hall systems, Phys. Rev. B **104**, 155307 (2021).

[34] Z.-Z. Chen, R. Lü, and B.-fen Zhu, Effects of electron-phonon interaction on nonequilibrium transport through a single-molecule transistor, Phys. Rev. B **71**, 165324 (2005).

[35] P. I. Arseev and N. S. Maslova, Electron-vibration interaction in tunneling processes through single molecules, Phys. Usp. **53**, 1151 (2010).

[36] J. Duan, F. J. Alfaro-Mozaz, J. Taboada-Gutiérrez, I. Dolado, G. Álvarez-Pérez, E. Titova, A. Bylinkin, A. I. F. Tresguerres-Mata, J. Martín-Sánchez, S. Liu, J. H. Edgar, D. A. Bandurin, P. Jarillo-Herrero, R. Hillenbrand, A. Y. Nikitin, and P. Alonso-González, Active and passive tuning of ultranarrow resonances in polaritonic nanoantennas, Adv. Mater. **34**, 2104954 (2022).

[37] S. Datta, Coherent transport, *Quantum Transport: Atom to Transistor* (Cambridge University Press, Cambridge, 2005), pp. 217–251.

[38] R. Landauer, Electrical resistance of disordered one-dimensional lattices, Philos. Mag. A **21**, 863 (1970).

[39] C. Caroli, R. Combescot, P. Nozieres, and D. Saint-James, Direct calculation of the tunneling current, J. Phys. C **4**, 916 (1971).

[40] See Supplemental Material at http://link.aps.org/supplemental/10.1103/PhysRevB.109.045432 for further examples of cavity-modified conduction at various disorder realizations.

[41] Increased strength of cavity effects at $\hbar\omega \to 0$ persists if only γ itself is independent of ω or decreases at larger ω. In fact, $\gamma \propto A_{\rm vac} \propto (\omega V)^{-1/2}$. Considering sequential modes of the same cavity, we see that the respective couplings γ indeed decay. Considering the fundamental modes of different cavities, we observe that $V \propto \lambda_0^3 \propto \omega^{-3}$. This results in growing $\gamma \propto \omega$.

[42] I. Epstein, D. Alcaraz, Z. Huang, V.-V. Pusapati, J.-P. Hugonin, A. Kumar, X. M. Deputy, T. Khodkov, T. G. Rappoport, J.-Y. Hong, N. M. R. Peres, J. Kong, D. R. Smith, and F. H. L. Koppens, Far-field excitation of single graphene plasmon cavities with ultracompressed mode volumes, Science **368**, 1219 (2020).

[43] L. B. Tan, O. Cotlet, A. Bergschneider, R. Schmidt, P. Back, Y. Shimazaki, M. Kroner, and A. İmamoğlu, Interacting polaron-polaritons, Phys. Rev. X **10**, 021011 (2020).

[44] B. Besga, C. Vaneph, J. Reichel, J. Estève, A. Reinhard, J. Miguel-Sánchez, A. Imamoğlu, and T. Volz, Polariton boxes in a tunable fiber cavity, Phys. Rev. Appl. **3**, 014008 (2015).